Research in Astron. Astrophys. **2012** Vol. **12** No. **6**, 678–692
http://www.raa-journal.org *http://www.iop.org/journals/raa*

Research in Astronomy and Astrophysics

The silicate and carbon-rich models of CoRoT-7b, Kepler-9d and Kepler-10b *

Yan-Xiang Gong[1,2] and Ji-Lin Zhou[1]

[1] Department of Astronomy & Key Laboratory of Modern Astronomy and Astrophysics in Ministry of Education, Nanjing University, Nanjing 210093, China; *zhoujl@nju.edu.cn*
[2] College of Physics and Electronic Engineering, Taishan University, Taian 271021, China

Received 2011 August 9; accepted 2012 February 11

Abstract Possible bulk compositions of the super-Earth exoplanets CoRoT-7b, Kepler-9d, and Kepler-10b are investigated by applying a commonly used silicate model and a non-standard carbon model. Their internal structures are deduced using a suitable equation of state for the materials. The degeneracy problems of their compositions can be partly overcome, based on the fact that all three planets are extremely close to their host stars. By analyzing the numerical results, we conclude: 1) the iron core of CoRoT-7b is not more than 27% of its total mass within 1σ mass-radius error bars, so an Earth-like composition is less likely, but its carbon rich model can be compatible with an Earth-like core/mantle mass fraction; 2) Kepler-10b is more likely to have a Mercury-like composition, with its old age implying that its high iron content may be a result of strong solar wind or giant impact; 3) the transiting-only super-Earth Kepler-9d is also discussed. Combining its possible composition with the formation theory, we can place some constraints on its mass and bulk composition.

Key words: planets and satellites: general — methods: numerical — planets and satellites: individual (CoRoT-7b, Kepler-9d, Kepler-10b)

1 INTRODUCTION

Rocky planets (like the Earth in our solar system) located in the habitable zone of their stars are presently the best candidates for harboring extra-terrestrial life (Léger et al. 2011). Therefore, the search for rocky exoplanets plays an important role in the detection of exoplanets. Recent observations of exoplanets have revealed 758 exoplanets (*http://exoplanet.eu/*, as of 2011 November 3), mainly through stellar radial velocity measurements or photometric detection of planets transiting their host stars. Among them, more than 30 exoplanets have a minimum mass of < 10 Earth masses ($M_\oplus$). They are called 'super-Earths' and a faction of them may possibly be rocky planets. Recently, the Kepler mission revealed 1235 planetary candidates with transit-like signatures detected during its first four months of operation (Borucki et al. 2011). Among them, 68 candidates are approximately Earth-sized ($R_\mathrm{p} < 1.25\,R_\oplus$), and 288 are super-Earth sized ($1.25\,R_\oplus < R_\mathrm{p} < 2\,R_\oplus$). Beyond all doubt, we are entering the era of small exoplanets. Some of them are expected to be terrestrial in nature.

∗ Supported by the National Natural Science Foundation of China.

Table 1 Planet parameters for Kepler-9d (Torres et al. 2011), Kepler-10b (Batalha et al. 2011), and CoRoT-7b (Léger et al. 2009). The ages of their host stars are also listed here.

Planet Name	Kepler-10b	Kepler-9d	CoRoT-7b
Mass ($M_\oplus$)	$4.56^{+1.17}_{-1.29}$	$3.5 - 7.0^{(a)}$	$4.8 \pm 0.8^{(b)}$
Radius ($R_\oplus$)	$1.416^{+0.033}_{-0.036}$	$1.64^{+0.19}_{-0.14}$	1.68 ± 0.09
Orbital Period (day)	$0.837495^{+0.000004}_{-0.000005}$	1.592851 ± 0.000045	0.853585 ± 0.000024
Equilibrium Temperature (K)	$1833^{(c)}$	2026 ± 60	1800–2600
Orbital Semimajor Axis (AU)	$0.01684^{+0.00032}_{-0.00034}$	$0.02730^{+0.00042}_{-0.00043}$	0.0172 ± 0.00029
Host Star Age (Gyr)	11.9 ± 4.5	3.0 ± 1.0	$1.5^{+0.8}_{-0.3}{}^{(d)}$

$^{(a)}$ Holman et al. (2010); $^{(b)}$ Queloz et al. (2009); $^{(c)}$ Calculated value – assuming a Bond albedo of 0.1 and a complete redistribution of heat for re-radiation; $^{(d)}$ *http://www.exoplanet.eu/*.

Understanding super-Earths is of great interest to us due to their possible rocky nature. What is the bulk composition of these new planets? How were they formed? These are all interesting yet puzzling questions. However, the information presently available based on observations for understanding their composition is still limited. Through transit and radial velocity detections, planetary radii and masses are the only windows presently available to investigate the composition of most exoplanets. Among the detected super-Earths, their masses and radii show quite different signatures when compared to the terrestrial planets found in our solar system. Their low average density tells us that they must primarily contain some light element that is lighter than water. They may have a significant gas envelope like Jupiter or Neptune in our solar system. However, super-Earths lacking gas envelopes, or 'rocky super-Earths,' may also be present in some cases, as we will discuss below.

CoRoT-7b is the first super-Earth with a measured radius, $R = 1.68 \pm 0.09\,R_\oplus$ (Léger et al. 2009). Its obtained mass derived from radial velocity measurements is $M = 4.8 \pm 0.8\,M_\oplus$ (Queloz et al. 2009). After 2009, the initial results were revised by other authors. For example, the revision of CoRoT-7's stellar parameter by Bruntt et al. (2010) yielded $M = 5.2 \pm 0.8\,M_\oplus$. Hatzes et al. (2011) performed another analysis of the data and obtained a larger mass, $M = 7.0 \pm 0.5\,M_\oplus$. Work undertaken by Boisse et al. (2011) and Ferraz-Mello et al. (2011) obtained different results. In this paper, we do not consider those masses but rather only use the initial data of CoRoT-7b. Recently, two transiting super-Earths, Kepler-9d (Torres et al. 2011) and Kepler-10b (Batalha et al. 2011) were also discovered. Kepler-9d was first discovered in 2010 as a planet candidate named KOI-377.03 (Holman et al. 2010). It was validated as a super-Earth and the reported radius is $R = 1.64^{+0.19}_{-0.14}\,R_\oplus$ (Torres et al. 2011). Although current spectroscopic observations are so far insufficient to establish its mass, a possible mass range can be found by Holman et al. (2010). The upper mass limit of $M = 7\,M_\oplus$ corresponds to the maximum mantle-stripping limit (Marcus et al. 2010) for a maximally iron-rich super-Earth. The lower mass limit is $\sim$3.5 $M_\oplus$ for a volatile-poor rocky planet with a Ganymede-like Fe/Si ratio. So we consider all possible compositions of Kepler-9d using this mass range. In this paper, we use Kepler-9d as an example to show what can be inferred for 'transiting-only' hot super-Earths. Kepler-10b was discovered in early 2011; the reported mass and radius are $M_\mathrm{p} = 4.56^{+1.17}_{-1.29}\,M_\oplus$ and $R_\mathrm{p} = 1.416^{+0.033}_{-0.036}\,R_\oplus$ (Batalha et al. 2011), respectively. The main parameters of these three exoplanets are summarized in Table 1.

The bulk composition of an exoplanet cannot be uniquely determined by the measured mass and radius. When more than two chemical constituents are taken into consideration, a measured radius and mass correspond to more than one possible bulk composition; in other words, it is a degeneracy problem. The degeneracy problems of bulk compositions of low-mass exoplanets can be partly overcome if they are very close to their host stars, because some chemical constituents may be ruled out a priori. Valencia et al. (2010) discussed the evolution of close-in low-mass planets like CoRoT-7b. Due to the intense stellar irradiation and its small size, it is unlikely to possess an

envelope of hydrogen and helium with more than 1/10 000 of its total mass. A relatively significant mass loss of $\sim 10^{11}$ g s^{-1} is expected and the result should prevail independently of the planet's composition; the hydrogen-helium gas envelope or water vapor atmosphere would escape within $\sim$1 Gyr, which is shorter than the calculated age of 1.2–2.3 Gyr for CoRoT-7b. The age of Kepler-9 is 3$\pm$1 Gyr and Kepler-10 is a relatively old star (11.9$\pm$4.5 Gyr), so volatile-rich solutions are less likely if the Kepler-9 and Kepler-10 planetary systems are old and evaporation has been substantial. Jackson et al. (2010) studied the coupling of tidal evolution and evaporative mass loss on CoRoT-7b. Their investigation indicated that the orbital decay caused by the star-planet tidal interaction enhanced its mass loss rate. Such a large mass loss also suggests that, even if CoRoT-7b began as a gas giant planet, its original atmosphere has now completely evaporated. Since both Kepler-9d and Kepler-10b are small close-in planets (with orbital periods 1.59 and 0.84 days, respectively), evaporation on the planets is serious due to high stellar irradiation. Thus, the origin of low-mass exoplanets, like Kepler-9d and CoRoT-7b, cannot be inferred from the present observations: they may have always had a rocky composition; they may be remnants of a Uranus-like ice giant, or a gas giant with a small core that has been stripped of its gaseous envelope (Valencia et al. 2010). The latest results from Leitzinger et al. (2011) indicated that hydrogen-rich gas giants within the mass domain of Jupiter and Saturn cannot thermally lose such an amount of mass that CoRoT-7b and Kepler-10b would result in a rocky residue. They also concluded that these planets were most likely always rocky planets.

In this paper, we assume that CoRoT-7b, Kepler-9d, and Kepler-10b do not have significant gas envelopes and consider them as being fully differentiated with all possible iron-to-silicate ratios. The differentiation assumption is not restrictive since all the terrestrial planets and some large satellites in the solar system are known to be differentiated. Using a relatively simple but well suited model for terrestrial planets in the solar system, we discuss the interior structures of CoRoT-7b, Kepler-9d and Kepler-10b. We compare the silicate model with the carbon model (Seager et al. 2007). Our main aims are: 1) infer their bulk composition and sharpen the observational constraints on their masses and radii, 2) compare their interior structures and infer some clues about their formation.

2 MODEL AND METHOD

2.1 Models and Numerical Method

If the rotation rate is not extreme, self-gravitating bodies are close to spherical. Spherical structures are certainly an adequate starting place for studies of exoplanets. Three equations must be satisfied. They are the equation of hydrostatic equilibrium-Equation (1), the mass conservation equation-Equation (2) and the equation of state (EOS)-Equation (3) for the material:

$$\frac{dP\,(r)}{dr} = -G\frac{m\,(r)\,\rho\,(r)}{r^2}\,, \tag{1}$$

$$\frac{dm\,(r)}{dr} = 4\pi r^2\rho\,(r)\,, \tag{2}$$

$$P\,(r) = f\,[\rho\,(r)\,,\ T\,(r)]\,, \tag{3}$$

where $m\,(r)$ is the mass contained within radius r, $P\,(r)$ is the pressure, $T\,(r)$ is the temperature, and $\rho\,(r)$ is the density of a spherical planet. The thermal contributions to the conclusion can be ignored, which has been tested in Seager et al. (2007) and this approximation has often been used in other works (Fortney et al. 2007; Léger et al. 2004). As a reasonable approximation, the temperature-independent EOS is also used in this work. If pressure is a nonlinear function of density, Equation (1) can be rewritten as

$$\frac{d\rho}{dr} = -G\frac{m\,(r)\,\rho\,(r)}{r^2}\cdot\frac{1}{dP\,(r)/d\rho\,(r)}\,. \tag{4}$$

We numerically integrate Equations (2) and (4) starting at the planet's center $r = 0$ while using the inner boundary conditions $m(0) = 0$ and $\rho(0) = \rho_{\rm c}$, where $\rho_{\rm c}$ is a chosen central density. For the outer boundary condition, we use $P(R_{\rm p}) = 0$. The choice of $\rho_{\rm c}$ at the inner boundary and the outer boundary condition $P(R_{\rm p}) = 0$ define the planetary radius $R_{\rm p}$ and total mass $M_{\rm p} = m(R_{\rm p})$. Integrating Equations (2) and (4) repeatedly for a range of $\rho_{\rm c}$ provides the mass-radius relationship (see Sect. 3.1.1) for a given material. For a differentiated model containing more than one kind of material, we specify the desired fractional mass of the core and of each shell. We then integrate Equations (2) and (4) as specified above, given a $\rho_{\rm c}$ and outer boundary condition. Using the planetary mass, we switch from one material to the next where the desired fractional mass is reached. Since we do not know the total mass that a given integration will yield ahead of time, we generally need to iterate a few times (change the value of $\rho_{\rm c}$) in order to produce a model with the desired distribution of material.

2.2 The Choice of the EOS

The materials used in this paper are ice VII, SiC, $MgSiO_3$ (enstatite, ab. en), $(Mg_{0.88}, Fe_{0.12})SiO_3$ (perovskite, ab. pv), Fe(α), and Fe(ε). Ice VII is used to model the ice composition in the large moons of giant planets. $MgSiO_3$ and $(Mg_{0.88}, Fe_{0.12})SiO_3$ are used to model the silicate mantles of terrestrial planets or large moons in our solar system. Enstatite is a low-pressure mineralogical phase of silicate, so it is only used for the validation of the model (see Sect. 3.1.2). Fe(α) and Fe(ε) are different phases of iron under different pressure, and Fe(ε) is the phase occurring at higher pressure. We compare their differences in terms of the mass-radius relation for homogeneous planets. For CoRoT-7b, Kepler-9d, and Kepler-10b, we use Fe(ε) to model their iron cores. Let us consider the range of pressure in our topic. $P_{\rm c}$, the central pressure of the planet, can be estimated as the following

$$P_{\rm c} \sim GM_{\rm p}^2/4R_{\rm p}^4 \,. \tag{5}$$

It is about 10^3 GPa for the three exoplanets. For $P \leq 200$ GPa, we use fits to the experimental data, using either the Vinet EOS (VE) Equation (6) or the Birch-Murnaghan EOS (BME) Equation (7). In general, when $P \geq 10^4$ GPa, where electron degeneracy pressure becomes increasingly important, the Thomas-Fermi-Dirac (TFD) theoretical EOS (Salpeter & Zapolsky 1967) must be employed, but this is out of the range we need. The pressure range, from approximately 200 to 10^3 GPa, is not easily accessible to experiment, nor is it well described by the TFD EOS (Seager et al. 2007). We simply use the VE or BME for all materials in this pressure regime.

For a derivation of these EOSs, see Poirier (2000). The VE is

$$P = 3K_0 \left(\frac{\rho}{\rho_0}\right)^{2/3} \left[1 - \left(\frac{\rho}{\rho_0}\right)^{-1/3}\right] \exp\left\{\frac{3}{2}\left(K'_0 - 1\right)\left[1 - \left(\frac{\rho}{\rho_0}\right)^{-1/3}\right]\right\}, \tag{6}$$

and the third-order finite strain BME is

$$P = \frac{3}{2}K_0 \left[\left(\frac{\rho}{\rho_0}\right)^{7/3} - \left(\frac{\rho}{\rho_0}\right)^{5/3}\right] \left\{1 + \frac{3}{4}\left(K'_0 - 4\right)\left[\left(\frac{\rho}{\rho_0}\right)^{2/3} - 1\right]\right\}. \tag{7}$$

Here ρ_0 is the reference density, $K_0 = -V(\partial P/\partial V)_{P=0}$ is the bulk modulus of the material, and $K'_0 = (\partial K/\partial P)_{P=0}$ is its pressure derivative. Their values for the materials used in this paper are summarized in Table 2. The VE is used for the ε-phase of iron because it is more suitable than the BME for extrapolation to high pressures (Poirier 2000). The third-order BME is used for other materials.

Table 2 Parameters for the Birch-Murnaghan EOS (BME) or Vinet EOS (VE) Fits

Material	K_0 (GPa)	K_0'	ρ_0 (kg m^{-3})	EOS	Reference
Ice VII	23.7 ± 0.9	4.15 ± 0.07	1460	BME	[1]
SiC	227 ± 3	4.1 ± 0.1	3220	BME	[2]
$MgSiO_3$ (en)	125	5	3220	BME	[2]
$(Mg_{0.88}, Fe_{0.12})SiO_3$ (pv)	266 ± 6	3.9 ± 0.04	4260	BME	[2, 3]
Fe(α)	162.5 ± 5	5.5 ± 0.8	7860	BME	[2]
Fe(ε)	156.2 ± 1.8	6.08 ± 0.12	8300	VE	[4]

References: [1] Hemley et al. (1987), [2] Ahrens (2000), [3] Knittle & Jeanloz (1987), [4] Anderson et al. (2001).

2.3 Carbon Model

There is an assumption used when modeling the interior structure of solid exoplanets: their constituents are similar to the terrestrial planets in our solar system. They have an iron core and a silicate envelope following a differentiated model. However, based on current observations, other possibilities cannot be ruled out. The facts tell us that there are large differences between extrasolar planets and planets in our solar system. For example, research about hot Jupiters tells us it is dangerous to assume that some planets can only form in a particular area. It is useful to take as broad a view as possible (Fortney et al. 2007). As another possible composition, Seager et al. (2007) presented the idea of carbon planets (see also Gaidos 2000). The planets in our solar system were formed in an environment where the carbon-to-oxygen ratio C/O = 0.5. Their bulk compositions were determined by the high-temperature chemical equilibrium in the protoplanetary disk. Silicates (i.e. Si-O compounds) are the dominant constituents in terrestrial mantles. However, in an environment where C/O $\gtrsim$ 1, the condensation sequence changes dramatically (Larimer 1975; Lewis 1974; Wood & Hashimoto 1993). As a result, the high-temperature condensates will be carbon-rich compounds. Kuchner & Seager (2005) have explored some planet-formation scenarios and they proposed that carbon planets composed largely of SiC or other carbides should form in such environments. A carbon-rich nebula created by the disruptions of carbon-rich stars or white dwarfs is a natural cradle for carbon planets, so planets around pulsars and white dwarfs are candidate carbon planets. For example, the planets around pulsar PSR1257+12 (Wolszczan & Frail 1992) may be carbon-rich exoplanets. In the well-known β Pictoris debris disk (Roberge et al. 2006), an exoplanet named β Pic b was discovered by Lagrange et al. (2009); it is most likely a carbon-rich planet because it is located in a carbon-rich environment. Carbon planets can also form in a local area enriched in C or depleted in H_2O in an otherwise solar abundant protoplanetary disk (Seager et al. 2007). Lodders (2004) suggested that the planetary embryo that grew into Jupiter may have formed in such a locally carbon-rich area, and that Jupiter's embryo was a carbon planet. In this paper, we also consider the carbon model for CoRoT-7b, Kepler-9d, and Kepler-10b, in which SiC is the major mantle constituent. The detailed formation scenarios for Earth-mass carbon planets can be referenced from Kuchner & Seager (2005), and the latest research about carbon-rich giant planets can be found in Madhusudhan et al. (2011).

3 NUMERICAL RESULTS

3.1 Validation in the Solar System

3.1.1 Planets in the mass-radius relationship diagram

A mass-radius diagram is a useful tool when inferring a planet's bulk composition. Building on the work done by Zapolsky & Salpeter (1969), we first consider planets of uniform composition. The positions of CoRoT-7b, Kepler-9d, and Kepler-10b in a mass-radius diagram can quickly tell us whether or not we can model them as solid planets. In Figure 1, the lines are curves of the mass-

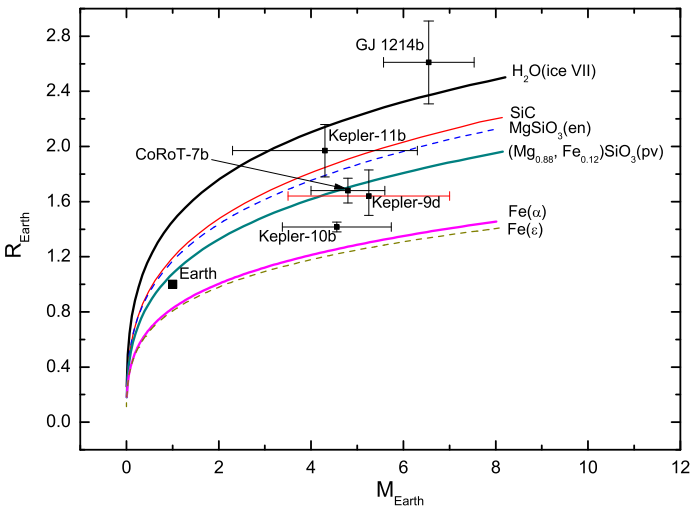

Fig. 1 Mass-radius relationship diagram for $M_{\rm p} \leq 10\,M_{\oplus}$. The solid or dashed lines are homogeneous planets. Five exoplanets and the Earth are marked on the diagram. The mass range of Kepler-9d (*red error bar; color online*) is taken from Holman et al. (2010). The locations of CoRoT-7b, Kepler-9d and Kepler-10b indicate that they can be described as solid planets.

radius relationship for homogeneous planets. From top to bottom, the homogeneous planets consist of ice VII, SiC, $MgSiO_3$ (enstatite, ab. en), $(Mg_{0.88}, Fe_{0.12})SiO_3$ (perovskite, ab. pv), Fe(α), and Fe(ε), respectively. Here, $MgSiO_3$ and $(Mg_{0.88}, Fe_{0.12})SiO_3$ are usually considered to be representative materials in a mantle. The phase diagram of iron in Valencia et al. (2010) can help us to understand the Fe(α) and Fe(ε) phases of iron (under different pressure ranges). CoRoT-7b, Kepler-9d, Kepler-10b and the Earth are marked on the mass-radius diagram. Two notable exoplanets, GJ 1214b (Charbonneau et al. 2009) and Kepler-11b (Lissauer et al. 2011), are introduced here for comparison. Their measured masses and radii tell us that Kepler-9d, Kepler-10b and CoRoT-7b are candidates of solid super-Earths. GJ 1214b is above the water ice VII line, which indicates that it must contain some light elements such as H and He; most likely it has a substantial gas envelope. Kepler-11b is above the solid SiC line, and it should have a substantial water vapor or H/He gas envelope because it is so close to its host star (10.3 days, Lissauer et al. 2011). As validation, we also mark some planets and satellites ($M \leq 1\,M_{\oplus}$) in our solar system in Figure 2. The Earth and Venus fall between the silicate and iron lines, but are closer to the silicate line, implying they contain more rock than iron. Ganymede is found between the silicate and the water ice VII lines, which indicates it must have significant amounts of ice in its composition. The Moon just lies on the silicate line, which is in agreement with the fact that the Moon is composed almost entirely of rock with a small iron core. Unlike the Moon, Mercury must have a massive iron core.

3.1.2 Code test for the differentiated planets

A mass-radius relationship diagram (or a one layer model) can only give us a qualitative estimation, but it cannot tell us the details of the interior structure. To estimate the precision of our code, we calculate the radii of the planets in a solar system from their total mass and mass fraction information published in the relevant literatures. On observation, the planet mass and radius uncertainties are typically 5% to 10% (Selsis et al. 2007), so a robust numerical code must guarantee that the error is less than 5%.

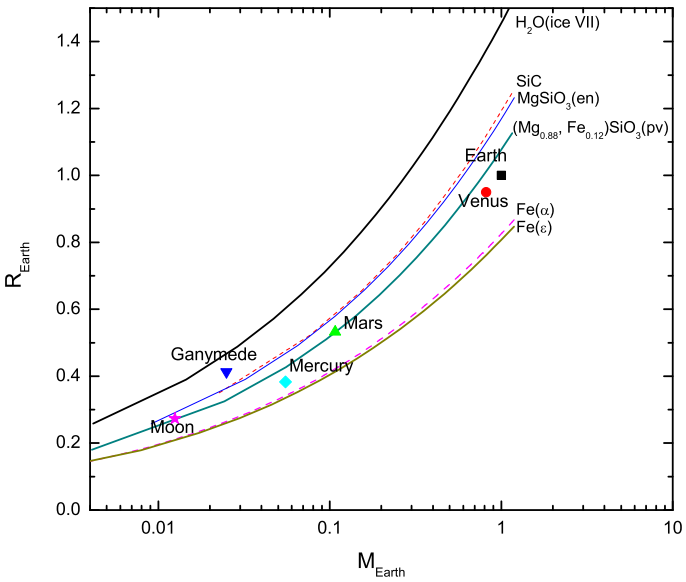

Fig. 2 Mass-radius relationship diagram for $M_{\rm P} \leq 1\,M_{\oplus}$. The solid or dashed lines are homogeneous planets. Various planets and satellites in the solar system are shown. Their major constituents can be estimated using this mass-radius diagram.

Table 3 Relative Error Between Calculated Radii and Actual Radii

Celestial Body Radius (km)[a]	Assumed Composition[b]	Model Radius (km)	Relative Error (%)
Mercury	60%Fe + 40%en	2474.43	1.40
2439.70	60%Fe + 40%pv	2344.78	3.80
Venus	27.9%Fe + 72.1%en	6283.54	3.83
6051.80	27.9%Fe + 72.1%pv	5862.68	3.13
Moon	3%Fe + 97%en	1745.05	0.43
1737.50	3%Fe + 97%pv	1652.37	4.90
Earth	32.5%Fe + 67.5%en	6589.91	3.40
6371.00	32.5%Fe + 67.5%pv	6269.81	1.59
Mars	20%Fe + 80%en	3409.08	0.58
3389.50	20%Fe + 80%pv	3149.51	7.00
Ganymede	6.5%Fe + 48.5%en + 45%ice VII	2525.19	4.02
2631.20	6.5%Fe + 48.5%pv + 45%ice VII	2454.14	6.73

[a] *http://ssd.jpl.nasa.gov/*; [b] References: Mercury, Solomon (2003); Venus, Zharkov (1983); Earth, Ganymede, Seager et al. (2007); Mars, Rivoldini et al. (2011).

Table 3 contains our obtained results. We must emphasize that the mass fractions of materials differ in the literature, which indicates that there are still some uncertainties in the bulk composition of solar system objects. For example, the iron core mass fraction of the Moon is estimated at less than 10% of its total mass – 3% is found by Canup & Asphaug (2001). We use both the pv and the en phases of silicate to calculate the radii, and the aim is only to test the model approach. Besides Ganymede and Mars (both having pv mantles), the relative error of all other planets and the Moon is less than 5%. A large relative error for Mars is understandable because Mars is relatively small, so

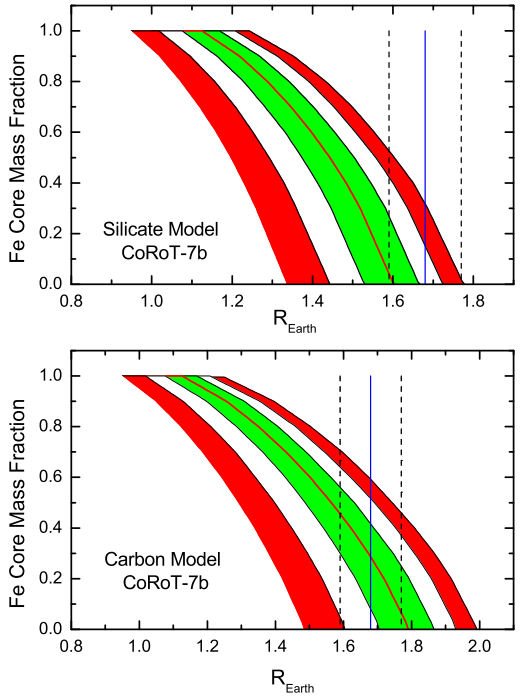

Fig. 3 Core mass fraction as a function of planetary radius for CoRoT-7b. The silicate model ($(Mg_{0.88}, Fe_{0.12})SiO_3$) and carbon model (SiC) are discussed. The planetary mass is $M = 4.8 \pm 0.8\, M_\oplus$. The green, white and red regions denote the core mass fractions obtained by varying its mass within 1σ, 2σ and 3σ error bars, respectively. The dashed black vertical lines delimit the measured radius $R = 1.68 \pm 0.09\, R_\oplus$. The Silicate model of CoRoT-7b had been discussed by Rogers & Seager (2010) and Valencia et al. (2010). We redo it for the comparison with its carbon model.

the pv is less suitable. Mercury is small too, but it has a large iron core, so pv or en cannot cause large discrepancies. The relatively large error (6.73%) of Ganymede (with a pv mantle) may be caused by the relatively low pressures in the deep interior of Ganymede (Sohl et al. 2002), and therefore pv is not very suitable either. The calculated Earth radius is within 101 km (only 1.59% error) of the actual Earth, which means that pv is the predominant mantle mineralogical phase in Earth.

3.2 The Results for Three Exoplanets

We examine the interior composition of Kepler-10b, Kepler-9d and CoRoT-7b under the assumption of an iron core covered by a mantle composed of $(Mg_{0.88}, Fe_{0.12})SiO_3$ (silicate model, similar to Earth's mantle) or SiC (carbon model). When considering two-layer models, the measured mass and radius uniquely determine the planet's composition. The core mass fraction as a function of planet radius for the three planets is displayed in Figures 3–5. The solid red line denotes the fraction of the planet's mass in its iron core according to an errorless planetary mass, while the green, white, and red shaded regions in Figures 3–4 delimit the 1σ, 2σ, and 3σ error bars of $M_{\rm p}$, respectively. In Figure 5, the solid red line denotes the iron core mass fraction for $M_p = 5.25\ M_\oplus$ (middle mass between 3.5–7.0 $M_\oplus$). The gray regions in Figure 5 delimit the mass range we considered. The measured

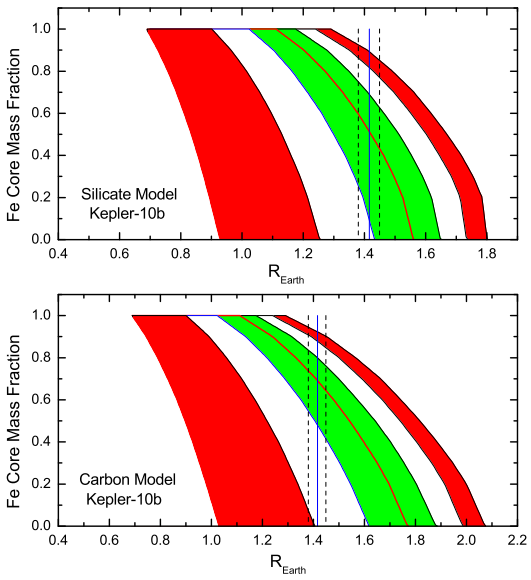

Fig. 4 Kepler-10b core mass fraction as a function of planetary radius. The silicate model ($(Mg_{0.88}$, $Fe_{0.12})$ SiO_3) and the carbon model (SiC) are discussed. The lines and areas are similar to Fig. 3. The planetary mass is $M = 4.56^{+1.17}_{-1.29}\ M_\oplus$ and the measured radius is $R = 1.416^{+0.033}_{-0.036}\ R_\oplus$. $\Delta M = \pm 1.29\ M_\oplus$ is used for 2σ and 3σ error bars of its mass.

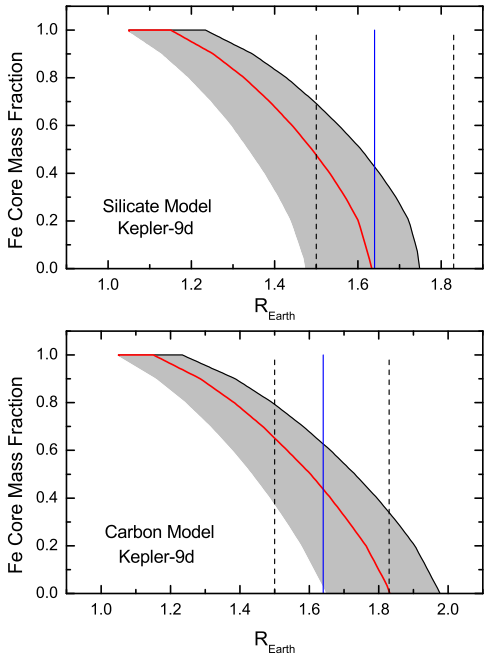

Fig. 5 Kepler-9d core mass fraction as a function of planetary radius. The silicate model ($(Mg_{0.88}$, $Fe_{0.12})$ SiO_3) and the carbon model (SiC) are discussed. The measured radius is $R = 1.64^{+0.19}_{-0.14}\ R_\oplus$. The gray region denotes the core mass fractions obtained by varying the mass within the mass range we considered, $M = 5.25 \pm 1.75\ M_\oplus$.

planet radius and its 1σ error bars are denoted by the solid blue and the dashed black vertical lines, respectively.

Interior structure models can strengthen the observational constraints on a planet's mass and radius (Rogers & Seager 2010). For example, with the assumption that planets do not have a significant water or gas layer, some of the mass-radius pairs within $M_{\rm p} \pm 1\sigma_M$ and $R_{\rm p} \pm 1\sigma_R$ (including the 0σ mass-radius pair) can be ruled out because they correspond to bulk densities that are lower than a pure silicate planet. These excluded mass-radius pairs would necessitate water (or some other component lighter than silicate). In Figure 3–5, all mass-radius pairs in the 1σ error bar (both mass and radius) compose an area. Here, we call them the ''effective area.''

For CoRoT-7b, if it has an Earth-like silicate mantle, its radius must be less than the measured value ($1.68\,R_\oplus$) and its mass has to be larger than the measured mass ($4.8\,M_\oplus$) within 1σ error bars, which implies an iron core mass fraction of less than $\sim 27\%$. Within its observational value, its radius is unlikely to be less than the reliable value if it formed in a carbon rich environment and has a Moon-like composition (where the iron content is below 10% in the carbon model). Its iron core is not heavier than $\sim 70\%$ of its total mass even at a 3σ error bar (see the carbon model in Fig. 3); it is the largest value for both models. The silicate model of CoRoT-7b with an Earth-like iron core mass fraction (32.5%) is not consistent with the measured mass and radius within 1σ. If its mass is ascertained within a 2σ or 3σ error bar (in the range obtained by Hatzes et al. 2011), CoRoT-7b can be consistent with an Earth-like composition. From Figure 3, we can clearly see that the ''effective area'' in the carbon model is much larger than that for the silicate model.

Kepler-10b tells us other information. For its carbon model, there is a lower iron mass fraction limit (about 41%) within the 1σ error bar (see the carbon model in Fig. 4). Kepler10 (7.4–16.4 Gyr) is older than CoRoT-7 (1.2–2.3 Gyr). If CoRoT-7b is differentiated as we assumed, Kepler-10b is more likely to be differentiated. This means that Kepler-10b may have a larger iron core. Our simulation indicates that Kepler-10b is denser than CoRoT-7b, but the detailed calculation can tell us more: if CoRoT-7b has a silicate mantle, whereas Kepler-10b formed under carbon-rich circumstances, the upper core mass fraction limit of CoRoT-7b ($\sim 27\%$) is below the lower core mass fraction limit (41% mentioned above) of Kepler-10b! With regard to Kepler-10b's carbon model, the upper limit of the iron core's mass fraction is $\sim 84\%$ (see carbon model in Fig. 4) within a 1σ error bar. This value is the largest in its two models and is larger than the suggested value of Mercury ($\sim 60\%$) – the densest planet in our solar system.

In Figure 6, we give the histograms of iron content for CoRoT-7b and Kepler-10b. The lower value we take comes from the planet formation scenario which we will discuss later. Regarding Kepler-10b, the silicate model is compatible with an Earth-like composition within the 1σ error bar, and the mass is about $3.27\,M_\oplus$ (lower limit of the observational value). The carbon model of Kepler-10b is not compatible with an Earth-like core/mantle mass ratio (32.5% in the core).

Kepler-9d is shown in Figure 5. The gray band denotes the planetary mass range we are considering. If the maximum mantle-stripping theory is true, the silicate model in Figure 5 tells us that Kepler-9d's radius cannot be larger than $\sim$1.75 $R_\oplus$. In detail, if it has an Earth-like core/mantle mass ratio, its radius is no more than $\sim$1.7 $R_\oplus$ with the silicate model. Despite the mass of a transiting-only super-Earth being unknown, model simulations give constraints on their possible masses. For example, if Kepler-9d has an Earth-like mantle composition (silicate model in Fig. 5), it has a lower mass limit according to its smallest possible radius, which is larger than the lower mass limit ($3.5\,M_\oplus$) discussed in Holman et al. (2010). An Earth-like core mass fraction and the lower limit of observational radius ($\sim$1.50 $R_\oplus$) yield a total mass of $\sim$4.1 $M_\oplus$. In the mass range discussed in this paper, the carbon model of Kepler-9d is compatible with an Earth-like core/mantle mass ratio in a large range of radius.

Other information can be read from Figures 3–5. For a given mass, the carbon model yields a larger radius than the silicate model. If the core is not pure iron but also contains a light element such as sulfur (in the Earth's core), all of the slantwise lines will sway to the right a little more (having

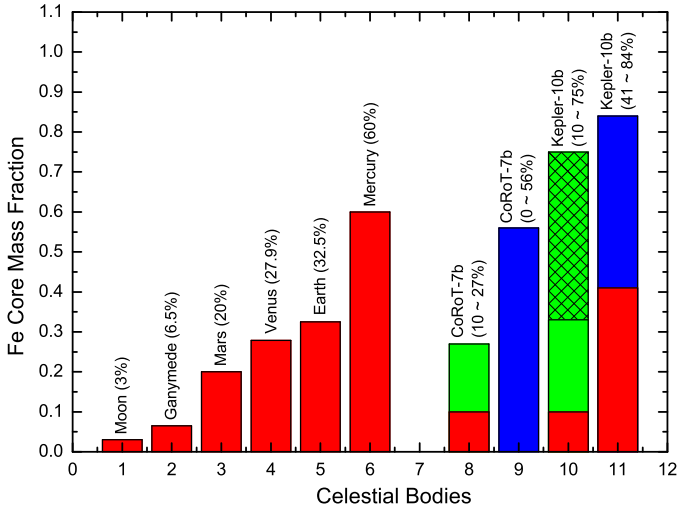

Fig. 6 The histograms of iron content for CoRoT-7b, Kepler-10b and the other celestial bodies mentioned in our work. The corresponding references are the same as in Table 3. The green part denotes the upper and lower limit for the silicate model, and the blue part denotes a similar limit for the carbon model (see details in Sect. 4). As for the grid range on the histogram of Kepler-10b (silicate model), the *lower* limit (33%) adopted by Marcus et al. (2010) is used. Obviously, from a statistical point of view, CoRoT-7b is compatible with a Mars-like core/mantle mass fraction, whereas Kepler-10b is compatible with a Mercury-like composition.

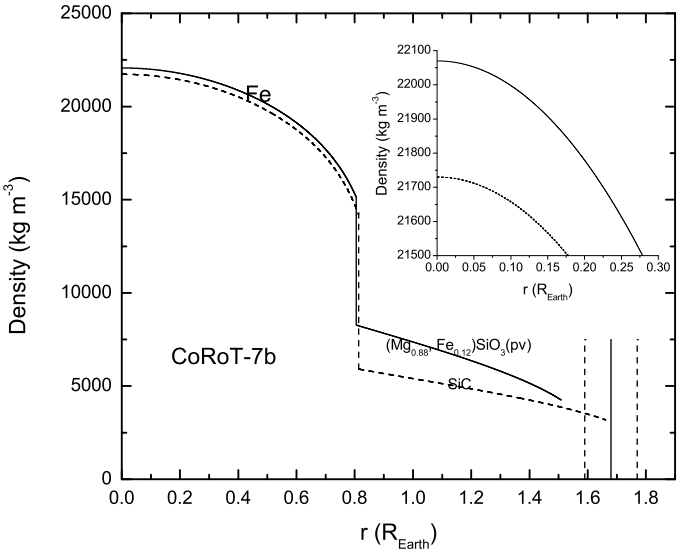

Fig. 7 The interior structure of CoRoT-7b. We use the reliable mass $M = 4.8\,M_{\oplus}$ with an Earth-like core/mantle mass ratio (iron core is 32.5%). Two mantle compositions are considered. The solid line is for $(Mg_{0.88}, Fe_{0.12})SiO_3$ and the dashed line is for SiC. Its radius range $R = 1.68 \pm 0.09\,R_{\oplus}$ is shown using vertical lines. The silicate model can be ruled out because the corresponding radius is out of the 1σ error bar for its reliable mass.

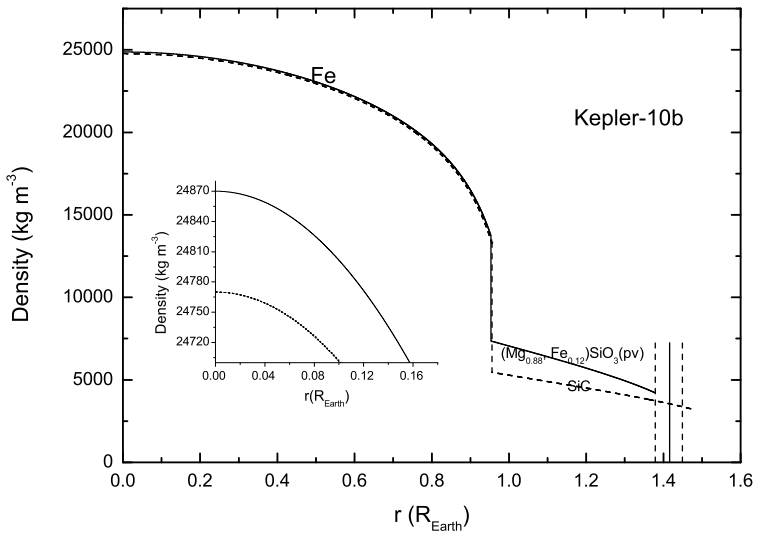

Fig. 8 The interior structure of Kepler-10b. We use a Mercury-like core/mantle mass ratio (iron core is 60%) and its reliable mass $M = 4.56\,M_{\oplus}$. Two mantle compositions are considered. The solid line is for $(Mg_{0.88}, Fe_{0.12})SiO_3$ and the dashed line is for SiC. Its radius range $R = 1.416^{+0.033}_{-0.036}\,R_{\oplus}$ is shown using vertical lines. The carbon model can be ruled out because the corresponding radius is out of the 1σ error bar for its reliable mass.

no effect on the radius at a core mass fraction of 0.0). This indicates that the core mass fraction at a specified planetary radius will be larger. Finally, we calculated the possible interior structure of CoRoT-7b and Kepler-10b using their presumable masses (Figs. 7–8). For CoRoT-7b, we take an Earth-like core/mantle mass ratio (core mass is 32.5%). From Figure 7, the silicate model of CoRoT-7b can be ruled out because the calculated radius is outside the observational 1σ error bar. For Kepler-10b, we take a Mercury-like core/mantle mass ratio (core mass is 60%). In Figure 8, Kepler-10b is compatible with a Mercury-like core/mantle mass ratio with its reliable mass for the silicate model.

4 DISCUSSION AND CONCLUSIONS

Two recently discovered super-Earths, Kepler-9d and Kepler-10b, and the previously found CoRoT-7b are discussed in this paper. Because of their intense irradiation and small size, gas envelopes are possibly absent. Under the assumption that they are mainly composed by refractory materials, their internal structures are deduced using a suitable equation of state for the materials. The silicate and the carbon models are discussed in detail. By analyzing the numerical results, we find that some of the mass-radius pairs within $M_{\rm p} \pm 1\sigma_M$ and $R_{\rm p} \pm 1\sigma_R$ can be ruled out. Therefore, our interior models sharpen the observational constraints on their masses and radii. For CoRoT-7b, an Earth-like composition with a silicate (pv) mantle is less likely within the 1σ error bars for both mass and radius, but a Mars-like composition may be suitable. For Kepler-10b's two models, a Mercury-like composition having 60% of its mass in an iron core is consistent with the measured mass and radius within a 1σ error bar. There is an upper and lower limit for the iron core mass fraction of every planet. Regarding CoRoT-7b, the upper iron core mass fraction limits are 27% (silicate model) and 56% (carbon model). For Kepler-10b, the silicate model has an upper limit of about 75% and its iron content is approximately $41\% \sim 84\%$ for the carbon model. A transiting-only exoplanet like

Kepler-9 can also be studied, for example, its radius is no more than 1.7 $R_\oplus$ in the silicate model. The lower mass limit (3.5 $M_\oplus$ we adopted) is also ruled out in its silicate model.

Our quantitative calculation tells us that Kepler-10b may be a Mercury-like planet. CoRoT-7b and Kepler-10b share similar features: radii, period, the type of host star and perhaps mass. Why is Kepler-10b denser than CoRoT-7b? Their different ages may give us some answers. For the anomalously dense case of Mercury in our solar system, there are three competing viewpoints (Solomon 2003): 1) the solar nebula caused aerodynamic drag on the particles from which Mercury was accreting, and iron and silicate have different responses to this drag, so the lighter particles were lost from the accreting material at the onset of accretion; 2) its surface rock could have been vaporized by strong radiation from a hot nebula and carried away by the solar wind; 3) much of the original crust and mantle has been stripped away by a giant impact caused by a planetesimal. Because of the lack of detailed observational data, which hypothesis is true cannot be determined. However, each hypothesis predicts a different surface composition. So two promising space missions currently underway, MESSENGER (Solomon et al. 2001, NASA) and the upcoming BepiColombo (Grard & Balogh 2001, ESA), could bring us the answer. The second and third explanations invoke processes late in the planetary accretion process, after the protoplanet had differentiated the silicate mantle from the metal core. If CoRoT-7b and Kepler-10b were born in a similar environment, Kepler-10b's abnormal iron content can be naturally associated with its older age. We think the postnatal alteration is more likely.

The lower limit of iron content of a super-Earth is an interesting question because a pure silicate super-Earth (iron mass fraction is zero) is unimaginable under the differentiation hypothesis. Under physically plausible conditions analogous to the solar system, planet formation will lead to a differentiated super-Earth with an iron core covered by a silicate mantle, with the proportions of each determined by the local Si/Fe ratio (Grasset et al. 2009). The only way to significantly increase the mean density of a planet requires the removal of an extended part of its silicate mantle. Marcus et al. (2010) proposed an efficient method – giant impacts between super-Earths. On the other hand, they prefer a lower limit of iron content of 33% by considering the standard cosmic abundances (see also Valencia et al. 2007). The initial Fe/Si ratio (average value) is used to give a lower limit for the iron content of a super-Earth. However, in practice, the process of formation must be influenced by other factors (such as the survival competition between planets) because some planets in a solar system have an iron content lower than this ''lower limit.'' We think that referring to the iron content in chondrites is a sound choice. L chondrites have lower total iron content, which is about 10% (Chen 2009). L chondrites are the largest group in the ordinary chondrites (40%, *http://www.nhm.ac.uk/*). Therefore, we use 10% as the lower limit for the silicate model. Regarding Figure 6, if there is a calculated lower limit of the iron content, we will use it, otherwise we use 10% (only for the silicate model).

Our main conclusions are summarized as follows: 1) the iron core of CoRoT-7b is not more than 27% of its total mass within 1σ mass-radius error bars, so an Earth-like composition is less likely, but its carbon rich model can be compatible with an Earth-like core/mantle mass fraction; 2) Kepler-10b is more likely to have a Mercury-like composition, and its old age implies that its high iron content may be a result of strong solar wind or a giant impact; 3) the transiting-only super-Earth Kepler-9d is also discussed. Combining its possible composition with the formation theory, we can place some constraints on the mass and composition of Kepler-9d. The radius derived from the transit method and the mass obtained by radial velocity detections together with the model simulation can constrain the possible compositions of exoplanets.

Credible conclusions desiderate comprehensive observations. Planetary formation theories, thermal evolution models, and studies of the cosmic abundance of elements can be used to place additional constraints on a planet's interior composition. Besides the temperature-independent model used in this paper, more complicated models of solid exoplanets can be found in other literatures. For example, Valencia et al. (2006) and Sotin et al. (2007) considered the temperature profile and

mixture of materials in the mantle or core. Wagner et al. (2011) used material laws in the infinite pressure limit to improve the model of solid exoplanets. In the near future, highly-sensitive spectroscopic transit observations of these exoplanets should constrain the compositions of the evaporating flow and therefore allow us to distinguish between rocky or gas-rich planets. In particular for exoplanets, without any opportunity for in situ composition measurements and gravitational moment measurements from spacecraft flybys, we will be permanently limited in what we can infer about the interior composition from their observed mass and radius (Rogers & Seager 2010).

Acknowledgements Firstly, we want to thank the anonymous referees for their constructive comments and suggestions, which improved the paper a great deal. This work was supported by the National Natural Science Foundation of China (Grant Nos. 10833001 and 10925313), Ph.D training grant of China (20090091110002), and Fundamental Research Funds for the Central Universities (No. 1112020102). Gong Yan-Xiang also acknowledges support from the Shandong Provincial Natural Science Foundation, China (ZR2010AQ023). We also thank Dr. Zeng Li from Harvard University for his communication with us about the interior structure of close-in exoplanets.

References

Ahrens, T. J. 2000, Mineral Physics & Crystallography: A Handbook of Physical Constants, vol. 2 (Washington, DC: AGU)
Anderson, O. L., Dubrovinsky, L., Saxena, S. K., & LeBihan, T. 2001, Geophys. Res. Lett., 28, 399
Batalha, N. M., Borucki, W. J., Bryson, S. T., et al. 2011, ApJ, 729, 27
Boisse, I., Bouchy, F., Hébrard, G., et al. 2011, A&A, 528, A4
Borucki, W. J., Koch, D. G., Basri, G., et al. 2011, ApJ, 736, 19
Bruntt, H., Deleuil, M., Fridlund, M., et al. 2010, A&A, 519, A51
Canup, R. M., & Asphaug, E. 2001, Nature, 412, 708
Charbonneau, D., Berta, Z. K., Irwin, J., et al. 2009, Nature, 462, 891
Chen, D. G. 2009, Geochemistry (Hefei: China Science and Technology Univ. Press) (in Chinese)
Ferraz-Mello, S., Tadeu Dos Santos, M., Beaugé, C., Michtchenko, T. A., & Rodríguez, A. 2011, A&A, 531, A161
Fortney, J. J., Marley, M. S., & Barnes, J. W. 2007, ApJ, 659, 1661
Gaidos, E. J. 2000, Icarus, 145, 637
Grard, R., & Balogh, A. 2001, Planet. Space Sci., 49, 1395
Grasset, O., Schneider, J., & Sotin, C. 2009, ApJ, 693, 722
Hatzes, A. P., Fridlund, M., Nachmani, G., et al. 2011, ApJ, 743, 75
Hemley, R. J., Jephcoat, A. P., Mao, H. K., et al. 1987, Nature, 330, 737
Holman, M. J., Fabrycky, D. C., Ragozzine, D., et al. 2010, Science, 330, 51
Jackson, B., Miller, N., Barnes, R., et al. 2010, MNRAS, 407, 910
Knittle, E., & Jeanloz, R. 1987, Science, 235, 668
Kuchner, M. J., & Seager, S. 2005, arXiv:astro-ph/0504214
Lagrange, A.-M., Gratadour, D., Chauvin, G., et al. 2009, A&A, 493, L21
Larimer, J. W. 1975, Geochim. Cosmochim. Acta, 39, 389
Léger, A., Grasset, O., Fegley, B., et al. 2011, Icarus, 213, 1
Léger, A., Rouan, D., Schneider, J., et al. 2009, A&A, 506, 287
Léger, A., Selsis, F., Sotin, C., et al. 2004, Icarus, 169, 499
Leitzinger, M., Odert, P., Kulikov, Y. N., et al. 2011, Planet. Space Sci., 59, 1472
Lewis, J. S. 1974, Science, 186, 440
Lissauer, J. J., Fabrycky, D. C., Ford, E. B., et al. 2011, Nature, 470, 53
Lodders, K. 2004, ApJ, 611, 587

Madhusudhan, N., Mousis, O., Johnson, T. V., & Lunine, J. I. 2011, ApJ, 743, 191
Marcus, R. A., Sasselov, D., Hernquist, L., & Stewart, S. T. 2010, ApJ, 712, L73
Poirier, J. P. 2000, Introduction to the Physics of the Earth's Interior (Cambridge: Cambridge Univ. Press)
Queloz, D., Bouchy, F., Moutou, C., et al. 2009, A&A, 506, 303
Rivoldini, A., van Hoolst, T., Verhoeven, O., Mocquet, A., & Dehant, V. 2011, Icarus, 213, 451
Roberge, A., Feldman, P. D., Weinberger, A. J., Deleuil, M., & Bouret, J.-C. 2006, Nature, 441, 724
Rogers, L. A., & Seager, S. 2010, ApJ, 712, 974
Salpeter, E. E., & Zapolsky, H. S. 1967, Physical Review, 158, 876
Seager, S., Kuchner, M., Hier-Majumder, C. A., & Militzer, B. 2007, ApJ, 669, 1279
Selsis, F., Chazelas, B., Bordé, P., et al. 2007, Icarus, 191, 453
Sohl, F., Spohn, T., Breuer, D., & Nagel, K. 2002, Icarus, 157, 104
Solomon, S. C. 2003, Earth and Planetary Science Letters, 216, 441
Solomon, S. C., McNutt, R. L., Gold, R. E., et al. 2001, Planet. Space Sci., 49, 1445
Sotin, C., Grasset, O., & Mocquet, A. 2007, Icarus, 191, 337
Torres, G., Fressin, F., Batalha, N. M., et al. 2011, ApJ, 727, 24
Valencia, D., Ikoma, M., Guillot, T., & Nettelmann, N. 2010, A&A, 516, A20
Valencia, D., O'Connell, R. J., & Sasselov, D. 2006, Icarus, 181, 545
Valencia, D., Sasselov, D. D., & O'Connell, R. J. 2007, ApJ, 665, 1413
Wagner, F. W., Sohl, F., Hussmann, H., Grott, M., & Rauer, H. 2011, Icarus, 214, 366
Wolszczan, A., & Frail, D. A. 1992, Nature, 355, 145
Wood, J. A., & Hashimoto, A. 1993, Geochim. Cosmochim. Acta, 57, 2377
Zapolsky, H. S., & Salpeter, E. E. 1969, ApJ, 158, 809
Zharkov, V. N. 1983, Moon and Planets, 29, 139